Supplementary Information

Electrode-Electrolyte Interactions Dictate Thermal Stability of Sodium-Ion Batteries

Susmita Sarkar, [a,b,‡] Avijit Karmakar, [a,‡] Bairav S. Vishnugopi, [a] Judith A. Jeevarajan, [c] and Partha P. Mukherjee [a,*]

[a]School of Mechanical Engineering, Purdue University, West Lafayette, IN 47907, USA

[b]Department of Mechanical and Aerospace Engineering, North Carolina State University, Raleigh, NC 27695, USA

[c]Electrochemical Safety Research Institute, UL Research Institutes, Houston, Texas 77204, USA

‡S.S and A.K share equal contribution.

S1. Experimental Methods

Materials:

The sodium (Na) metal, micro (μ) and nano (n) tin (Sn) metal powder, sodium perchlorate ($NaClO_4$), ethylene carbonate (EC), diethyl carbonate (DEC), propylene carbonate (PC), fluoroethylene carbonate (FEC), carboxymethyl cellulose (CMC) binder chemicals originated from Sigma-Aldrich Corporation. Sn electrodes with 70 wt.% Sn, 11 wt.% CMC binder and 19 wt.% carbon black (Super C65-TIMCAL) are prepared in the conventional slurry method using deionized (DI) water and ethanol as solvents. The sodium vanadium phosphate, $Na_3V_2(PO_4)_3$ (NVP) electrodes are prepared through a process similar to that of Sn electrodes with the NVP powder from MTI Corporation.

The thickness of the NVP cathode was approximately 80 μm, while the Sn anode had a thickness of approximately 20 μm after drying. The loadings of NVP for all tested electrodes were in the range of 8.02 ± 0.56 mg/cm². The Sn loadings for all tested electrodes were 1.75 ± 0.12 mg/cm² for micro-Sn and 2.05 ± 0.25 mg/cm² for nano-Sn, respectively.

The electrolytes consisted of 1 M $NaClO_4$ in a mixture of EC, DEC and PC (1:1:1 vol%) (Base). The fluoroethylene carbonate (FEC) was added as an electrolyte additive by incorporating 2 vol% FEC into the electrolyte mixture (Base+FEC).

To ensure a controlled environment, all electrolyte preparations were carried out in an argon-filled glove box with an oxygen and water content below 0.1 ppm.

Electrochemical Testing:

The CR2032 coin-type cells were used for electrochemical measurements. The Sn-based half cells were created by utilizing the Sn electrode as the working electrode and Na metal as the counter electrode. Similarly, NVP-based half cells were created by utilizing the NVP electrode as the working electrode and Na metal as the counter electrode. The full cell was assembled using NVP as the cathode and Sn as the anode, with Whatman GF/C as the separator in an argon-filled glove box to ensure an inert environment with oxygen and moisture levels below 0.1 ppm. Charge–discharge measurements were conducted across a voltage range of 3.8–2 V at a C/20 rate at room temperature (25°C). Two different electrolytes were used for the electrochemical tests: the first one being $NaClO_4$:EC:PC:DEC (Base) electrolyte without any additive and another being Base + FEC electrolyte with 2 vol% fluoroethylene carbonate (FEC) as an electrolyte additive to investigate the impact of FEC on cycling performance and thermal behavior of the full-cells.

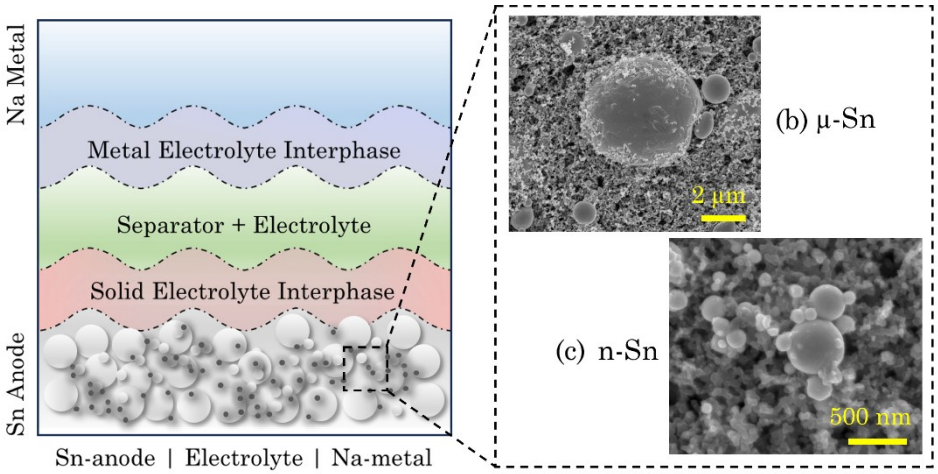

Figure SF1. The electrode/electrolyte interface can evolve depending on the electrolyte recipe and play a crucial role in determining the thermal stability of the system. (a) Schematic diagram of the used cell setup (Sn|Na) for ARC with the corresponding interphases. SEM image of the (b) µ-Sn and (c) n-Sn based electrode.

Accelerating Rate Calorimetry (ARC) Testing:

The Sn-based and NVP-based half cells and Sn-NVP-based full cells were subjected to heat-wait-seek (HWS) tests using EV+ ARC manufactured by Thermal Hazard Technology (THT). Four identically cycled coin cells were stacked together to achieve enough thermal mass to detect the

exothermic reactions. The parameters of the ARC experimental setup are summarized in Table ST1.

Table ST1. ARC testing parameters for the HWS method.

Descriptions	Values
Start temperature of the heat-wait-seek process [°C]	50
End temperature of the heat-wait-seek process [°C]	300
Temperature step of the heat-wait-seek process [°C]	5
Temperature rate sensitivity [°C/min]	0.02
Wait step time [min]	20

Table ST2. Characteristics temperatures for thermal runaway in ARC setup.

Symbol	Definition	Threshold
T_1	Onset temperature of self-heating	Temperature rate in the seek phase is greater than 0.02°C/min
T_2	Onset temperature of thermal runaway	Temperature rate in the adiabatic phase is greater than 1.0°C/min
T_3	Maximum temperature of thermal runaway	Peak temperature in adiabatic phase
$(dT/dt)_m$	Maximum self-heating rate	Maximum value of the temperature rate during the adiabatic phase
t_2-t_1	Time to onset of thermal runaway	Time required from T_1 to T_2

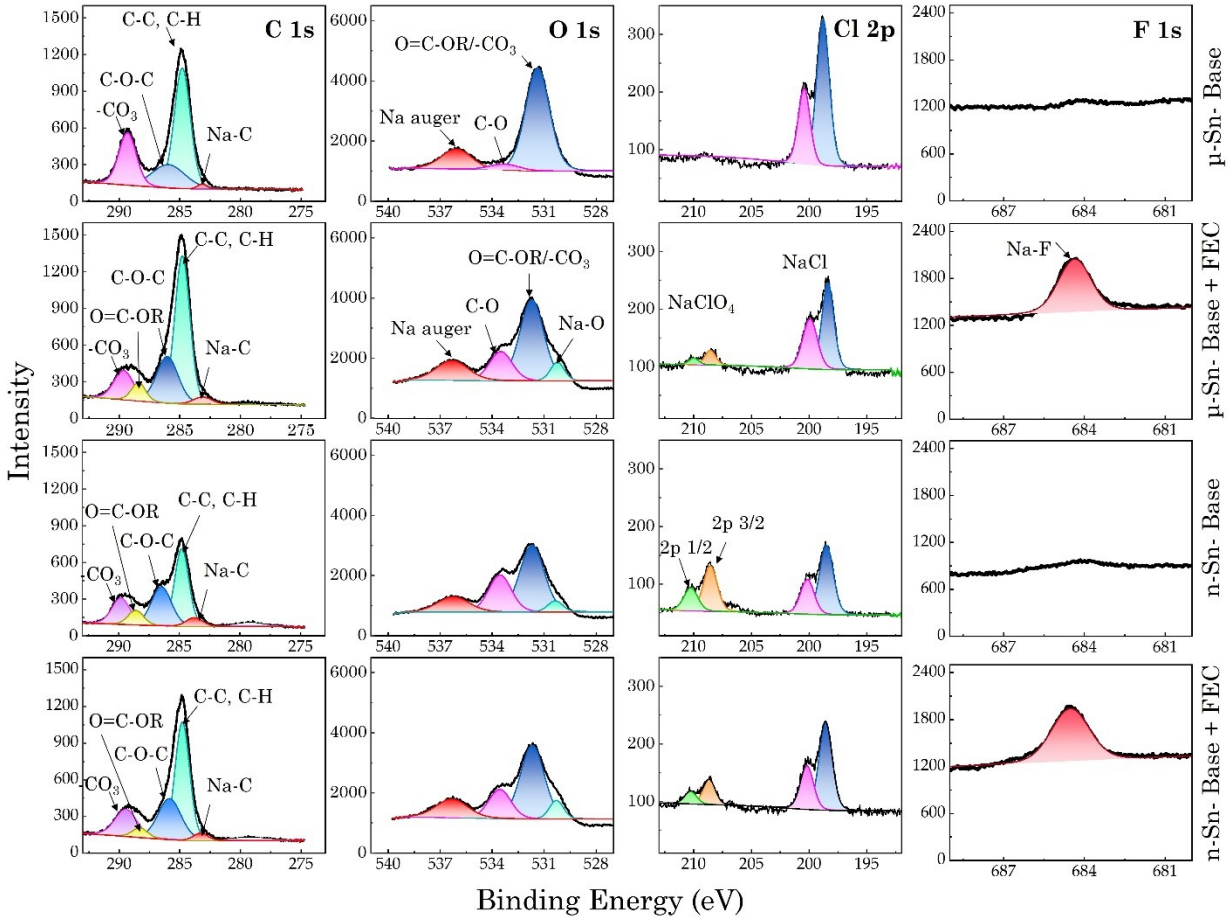

Figure SF2. XPS analysis of μ-Sn and n-Sn electrode post-cycled using the electrolytes of EC:PC:DEC – Base and EC:PC:DEC:FEC - Base + FEC.

Figure SF2 displays the spectra for different elements in the solid electrolyte interphase (SEI). In the μ-Sn electrode immersed in the Base electrolyte, the C 1s peak was deconvoluted into four distinct components, namely Na-C (at ~283 eV), C-C (at ~284.8 eV), C-O-C (at ~286 eV), and -CO3 (at ~289.3 eV). The Na-C peak suggests interactions between sodium and carbon species, likely originating from electrolyte reduction products. The C-C peak reflects carbon-carbon bonding from organic decomposition products, while the C-O-C and -CO_3 components correspond to ether groups and carbonate species, respectively.

When μ-Sn was exposed to an FEC-containing electrolyte, a new component emerged at 288.4 eV, indicating the presence of O=C-OR. Additionally, the FEC addition led to an increased concentration of C-O-C groups, implying enhanced formation of polymeric or ether-based compounds, while the concentration of carbonate species (-CO_3) decreased. This shift indicates

that FEC alters the SEI composition, reducing the amount of inorganic carbonate formation, which could affect the SEI's mechanical and chemical stability. FEC molecules preferentially decompose over other solvation species due to their enhanced ability to accept additional electrons. This is illustrated by FEC's involvement in the solvation sheath, where the spin electron either localizes on the O=CO(O) moiety or is shared between Na^+ and its C=O bond.

In the case of n-Sn, both the Base electrolyte and the Base + FEC electrolyte exhibited five distinct components. Notably, the concentrations of C-C and C-H increased, while the concentration of O-C-OR rose when FEC was introduced into the nano-sized Sn electrode. In the Base electrolyte, the O 1s component in the μ-Sn electrode exhibited a notable presence of O=C-OR/CO3 at ~531.4 eV, along with a minimal amount of C-O at ~533.3 eV. The final peak at ~536 eV was attributed to Na Auger. After adding FEC to the Base electrolyte, an additional peak at 530.2 eV, associated with Na-O, emerged.

Also, a decreased amount of -CO3 and an increase in C-O were observed for μ-Sn in FEC-based electrolytes. Conversely, for the n-Sn case, an inverse trend can be observed. The Base electrolyte showed a higher C-O concentration than the FEC-added electrolyte. Moreover, the amount of Na-O increased when FEC was introduced into the Base electrolyte for the n-Sn electrode. In the Cl 2p spectrum, only NaCl was detected on the surface due to the electrochemical reduction of NaClO4 salt. However, trace amounts of NaClO4 were also identified on the surface in the other three cases. When using an electrolyte containing FEC, a prominent peak at ~684.4 eV was observed in the F 1s spectra for both the μ-Sn and n-Sn. However, this peak was not present in the Base electrolyte. The emergence of this peak can be attributed to the decomposition of the FEC. Increased FEC concentration intensifies the SEI's inorganic components, particularly NaF and Na_2O, aligning with calculations showing coordinated FEC undergoes rapid defluorination with minimal activation energy.

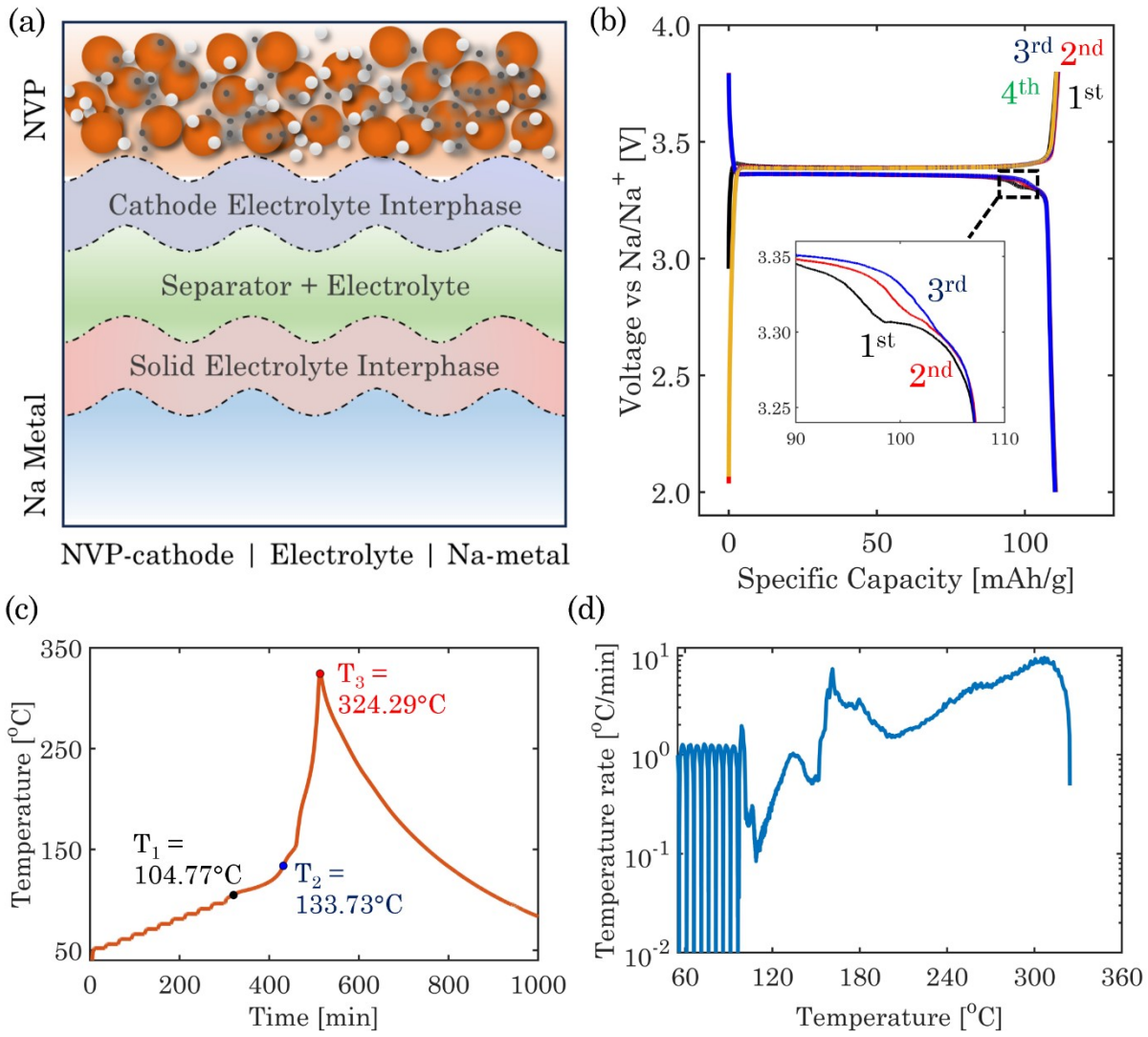

Figure SF3. (a) Diagrammatic representation of the employed cell configuration (NVP|Na) for ARC. (b) Voltage profile of NVP-Na metal-based half-cell. ARC experiments to probe the thermal stability of the NVP cathode. (c) Temperature response, and (d) the temperature increase and the corresponding self-heating rate of NVP-based half-cell. The selected electrolyte is $NaClO_4$:EC:PC:DEC:FEC (Base + FEC) electrolyte.

Figure SF3a shows the schematic representation of the NVP-based half-cell with counter electrode Na metal in Base + FEC electrolyte. The voltage response of the NVP electrode between 2.0-3.8V at a C-rate of C/20 for three charge-discharge cycles followed by a 4th charge is shown in Figure SF3b. The cell shows 1st charge capacity of 110.61 mAh/g and 1st discharge capacity of 110.37 mAh/g. The charge-discharge profile exhibits a remarkably steady voltage plateau at around 3.4

V, attributed to the V^{3+}/V^{4+} redox couple and indicative of the $Na_3V_2(PO_4)_3$ to $NaV_2(PO_4)_3$ transition reaction. The 2nd and 3rd discharges did not exhibit significant capacity loss, except that the plateau around 3.31 V increased to a slightly higher voltage from the 1st discharge. The thermal response of the NVP-based half-cell obtained from the ARC testing is depicted in Figure SF3c-d. The self-heating onsets at T_1 = 104.77°C, thermal runaway occurs at T_2 = 133.73°C, and the peak temperature recorded is T_3 = 324.29°C. The peak heating rate was around 9.51°C/min, with the time to thermal runaway being 111.01 min.

Electrochemical and Thermal stability of NVP-Sn full-cell

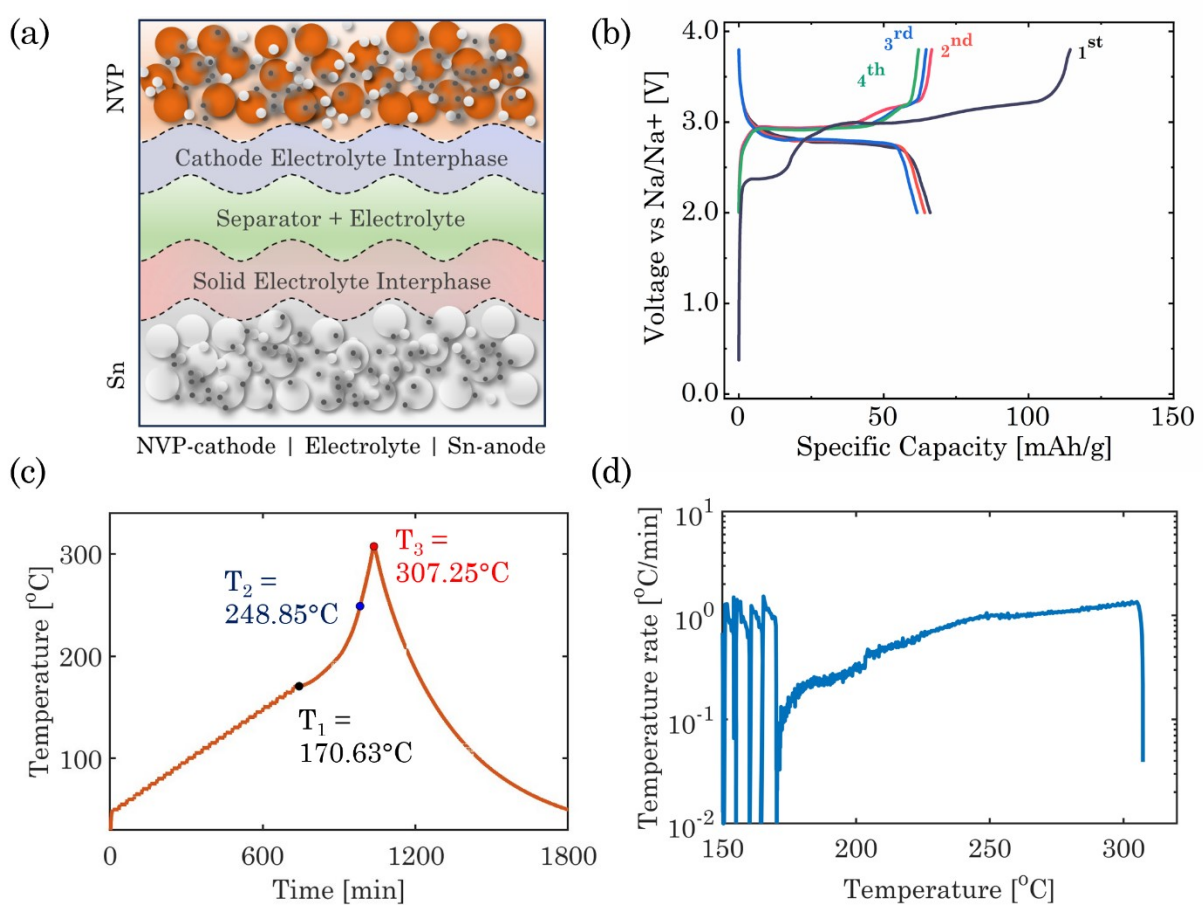

Figure SF4. The (a) Pictorial representation and (b) Voltage profile of the NVP-µ-Sn based full cell. ARC experiments to probe the thermal stability of the full cell. (c) ARC temperature response and (d) the temperature increase and the corresponding self-heating rate of NVP-µ-Sn-based full cell using the Base + FEC electrolyte.

Figure SF4a shows the schematics of the SIB full-cell based on the NVP cathode and Sn anode accompanied by the electrode-electrolyte interphases, which play a pivotal role in determining the electrochemical and thermal stability. Before performing the ARC study, the NVP-Sn-based full cells were cycled at C/20 for 3 cycles. Figure SF4b depicts the electrochemical operation of the SIB full cell in the voltage range between 2.0 and 3.8V. The 1st charging shows excellent capacity, almost close to the theoretical capacity of NVP. The 2nd cycle shows significant capacity loss from the 1st cycle, which can be attributed to the formation of an unstable SEI layer on Sn containing NaF species under FEC decomposition effects, leading to the consumption of sodium ions. The full cells depict very little capacity loss from the 2nd cycle onwards. The ARC thermal signature for the μ-Sn | Base + FEC | NVP full-cell is shown in Figure SF4c-d. It shows a self-heating onset at 170.63°C (T_1) and thermal runaway at 248.85°C (T_2). Beyond this limit, the self-heating rate initially slows down slightly and then increases rapidly (up to 1.3560°C/min), resulting in an exotherm and a maximum temperature of 307.25°C (T_3).

S2. Computational Methods

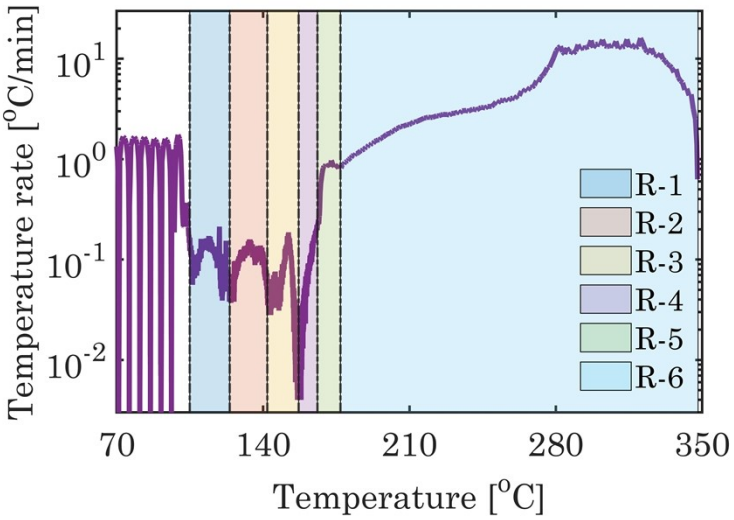

Figure SF5. Segmentation of the ARC thermal signature for n-Sn | Base + FEC | Na sample into different stages.

The segmentation of the ARC thermal signature for the n-Sn | Base + FEC | Na sample based on the change in temperature rate is shown schematically in Figure SF5. Each stage's start and end temperatures correspond to the start and end temperatures of each specific chemical reaction during the adiabatic phase of the ARC thermal signatures. For the n-Sn | Base + FEC | Na sample,

the primary SEI decomposition followed by interaction between decomposed SEI and Base + FEC electrolyte, denoted by R-1, starts at 104.94°C and ends at 124.02°C. The interaction between the decomposed SEI and molten Na, denoted by R-2, starts at 124.02°C and ends at 142.00°C. The reaction R-3, representing the interaction between the molten Na and Base + FEC electrolyte, starts at 142.00°C and ends at 157.00°C. The secondary SEI decomposition, followed by interaction between SEI products and Base + FEC electrolyte, denoted by R-4, initiates at 157.00°C and ends at 166.00°C. The n-Sn anode and the Base + FEC electrolyte interaction, denoted by R-5, start at 166.00°C and end at 177.00°C. Finally, the Base + FEC electrolyte decomposition and combustion, denoted by R-6, starts at 177.00°C and ends at 347.73°C. A similar segmentation of the ARC thermal signature of the other cell samples has been performed, which is reported in Table ST3.

Table ST3. Exothermic reactions for Sn-based half-cells under ARC heating tests.

Reactions	Description	Cell type	T_{start} [°C]	T_{end} [°C]
R-1	Primary solid electrolyte interphase (SEI) decomposition followed by interaction between decomposed SEI and electrolyte	µ-Sn | Base | Na	102.39	104.79
		µ-Sn | Base + FEC | Na	102.21	119.29
		n-Sn | Base | Na	76.82	97.36
		n-Sn | Base + FEC | Na	104.94	124.02
R-2	Interaction between decomposed SEI and molten Na	µ-Sn | Base | Na	112.01	113.26
		µ-Sn | Base + FEC | Na	102.21	119.29
		n-Sn | Base | Na	97.36	108.57
		n-Sn | Base + FEC | Na	124.02	142.00
R-3	Interaction between molten Na and electrolyte	µ-Sn | Base | Na	118.19	134.88
		µ-Sn | Base + FEC | Na	136.76	137.49
		n-Sn | Base | Na	108.57	129.22
		n-Sn | Base + FEC | Na	142.00	157.00
R-4	Secondary SEI decomposition, followed by interaction between SEI products and electrolyte	µ-Sn | Base | Na	157.11	166.31
		µ-Sn | Base + FEC | Na	161.36	168.18
		n-Sn | Base | Na	152.26	160.89
		n-Sn | Base + FEC | Na	157.00	166.00
R-5	Sn anode – electrolyte reaction	µ-Sn | Base | Na	166.31	215.46
		µ-Sn | Base + FEC | Na	168.18	198.84
		n-Sn | Base | Na	169.10	200.01
		n-Sn | Base + FEC | Na	166.00	177.00
R-6	Electrolyte decomposition and combustion	µ-Sn | Base | Na	215.46	311.39
		µ-Sn | Base + FEC | Na	198.44	313.27
		n-Sn | Base | Na	200.01	320.76
		n-Sn | Base + FEC | Na	177.00	347.73

Base electrolyte: $NaClO_4$:EC:PC:DEC Base + FEC electrolyte: $NaClO_4$:EC:PC:DEC:FEC

S2.1 Extraction of kinetic parameters from ARC profiles

The kinetic parameters of each exothermic reaction can be extracted by delineating the ARC temperature profile as $ln\left[\frac{dT}{dt}\Big/(T_e - T(t)\right]$ Vs. $1/T(t)$ and then applying the linear regression to it. The following Equation S1 can correlate the slope and intercept of the regression curve with the activation energy and frequency factor of the reaction, while the enthalpy change needs to be solved separately using Equation S2 by estimating the specific heat capacity of the reactant.

$$\left[\frac{\frac{dT(t)}{dt}}{(T_{e,i} - T(t))}\right] = ln[A_{m,i}] - \frac{E_{a,i}}{RT(t)} \#(S1)$$

$$H_i = C_{p,i}(T_{e,i} - T_{s,i}) \#(S2)$$

Here, A_m is the frequency factor, E_a is the activation energy, R is the universal gas constant, H is the reaction enthalpy, C_p is the specific heat capacity, T_s denotes the start temperature of the exothermic reaction, T_e denotes the end temperature of the exothermic reaction, and the subscript i denotes the reaction number.

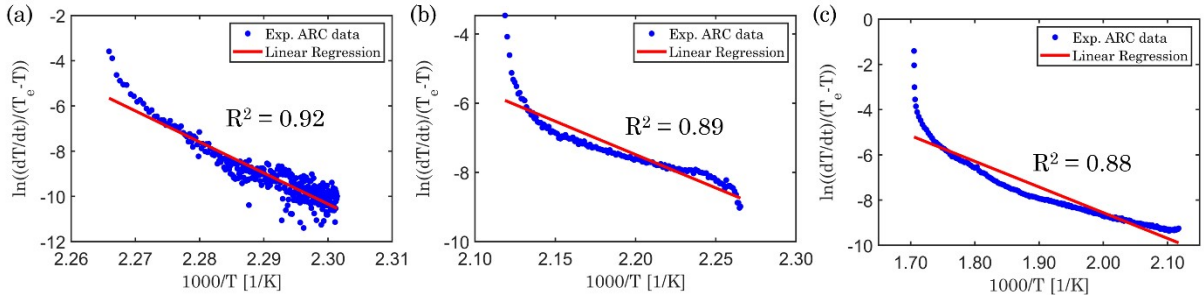

Figure SF6. Linear regression results of µ-Sn and Base + FEC electrolyte based exothermic reactions.

Table ST4. Kinetic parameters of µ-Sn and Base + FEC electrolyte based exothermic reactions.

Reactions	A_m (1/s)	E_a (J/mol)	H (J/g)
Secondary SEI decomposition	1.1334×10^{124}	1.0697×10^{6}	4.1653

Sn anode – electrolyte reaction	1.4272×10^{15}	1.6017×10^{5}	18.7298
Electrolyte decomposition	1.4067×10^{6}	9.4435×10^{4}	69.8824

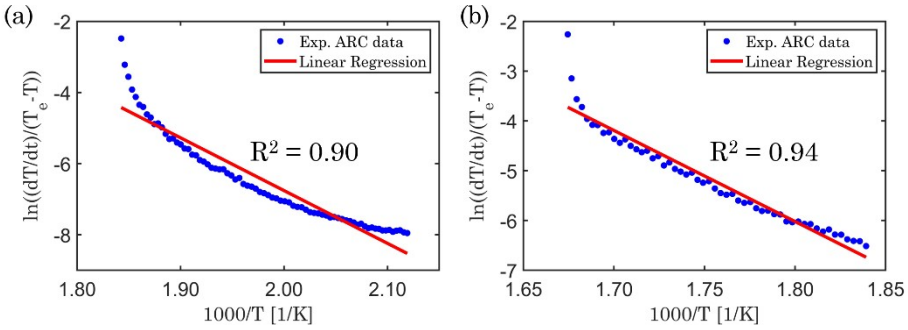

Figure SF7. Linear regression results of μ-Sn and Base + FEC electrolyte based exothermic reactions.

Table ST5. Kinetic parameters of NVP and Base + FEC electrolyte based exothermic reactions.

Reactions	**A_m (1/s)**	**E_a (J/mol)**	**H (J/g)**
NVP – electrolyte reaction	9.0660×10^{9}	1.2342×10^{5}	43.8499
Electrolyte decomposition	4.7923×10^{11}	1.5204×10^{5}	32.6421

S2.2 Virtual ARC model

The thermokinetics of the half-cell responses are used to predict the cell-level heat generation rate under an ARC setting using the following equations:

$$\dot{Q}_{gen}(t) = \sum_{i=1}^{n} m_i H_i \frac{dc_i(t)}{dt} = \sum_{i=1}^{n} m_i H_i A_{m,i} exp\left(-\frac{E_{a,i}}{RT(t)}\right) f[c_i(t)] \#(S3)$$

where $\dot{Q}_{gen}(t)$ denotes the net heat generation rate, m is the reactant mass, $c(t)$ denotes the reactant concentration and $f[c_i(t)]$ represents the mechanism function, and n denotes the total number of exothermic reactions. The cell temperature response for the ARC model follows the fundamental energy conservation equations given by,

$$MC_p \frac{dT(t)}{dt} = \dot{Q}_{gen}(t) - hA[T(t) - T_{ARC}(t)] \#(S4)$$

Here, M is the cell mass, h_{ARC} is the overall heat transfer coefficient (both convection and radiation) between the cell and the ARC chamber, S is the surface area of the cell, and $T_{ARC}(t)$ denotes the instantaneous temperature of the ARC chamber. The computational model employs a lumped thermal energy equation as the overall Biot number (a dimensionless number representing the ratio of internal thermal resistance to external thermal resistance) of a symmetrically placed pouch cell is generally small under the ARC setup, and a uniform temperature can be assumed throughout the entire cell without any significant internal temperature gradient. Under this assumption, the present study does not consider the effect of the different test positions on the thermal stability of the pouch cells in the virtual ARC setting. The mass of the cell components are 0.009 gm for the NVP cathode, 0.0035 gm for the Sn anode, 0.22 gm for the Base + FEC electrolyte. The total mass of the μ-Sn-NVP based full cell is 3.7 gm and the cell-level specific heat capacity is estimated to be 0.61 J/g-K.

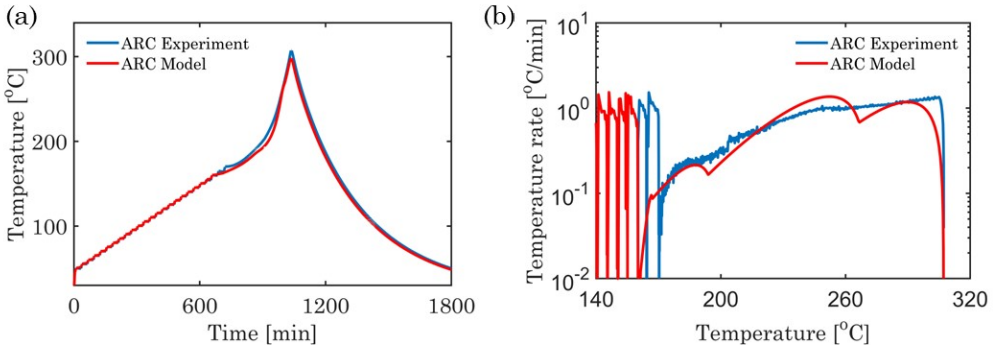

Figure SF8. Cell-level ARC simulations results. (a) Temperature vs. time profiles. (b) Temperature rate vs temperature profiles.

S2.3 Virtual Oven Test Model

Under oven conditions, the energy balance equation for the Li-ion pouch cell consists of the exothermic heat generation and heat dissipation to the surroundings. Therefore, we have,

$$MC_p\frac{dT(t)}{dt} = \dot{Q}_{gen}(t) - h_{oven}S[T(t) - T_{oven}] \#(S5)$$

where T_{oven} denotes the surrounding temperature in the oven, and h_{oven} denotes the overall heat transfer coefficient, representing the combination of convection and radiation effects. Therefore,

$$h_{oven} = h_{convection} + 4\varepsilon\sigma T_{oven}^{3} \#(S6)$$

where ε is the emissivity of the cell, and σ is the Stefan-Boltzmann constant. The convection heat transfer coefficient is assumed to be 5 W/m^2-K, and the cell emissivity is assumed to be 1.0. The mass of the pouch cell under varying capacities is reported in Table ST6.

The mass ratios of the electrodes (anode, cathode) and electrolytes in the full cells have been utilized to calculate the mass of the different components of the pouch cells with capacities ranging from 1 – 5 Ah and have been tabulated in Table ST6. The mass of the rest of the cell components is assumed to be constant across different capacities.

Table ST6. Mass of cell components for evaluating thermal stability of cell-level SIBs under oven conditions.

Capacity (Ah)	m_{anode} (g)	$m_{cathode}$ (g)	$m_{electrolyte}$ (g)	m_{rest} (g)	m_{cell} (g)
1.0	1.18	8.33	3.91	10.00	23.42
2.0	2.36	16.67	7.83	10.00	36.86
3.0	3.54	25.00	11.75	10.00	50.29
4.0	4.72	33.33	15.67	10.00	63.72
5.0	5.90	41.67	19.58	10.00	77.15

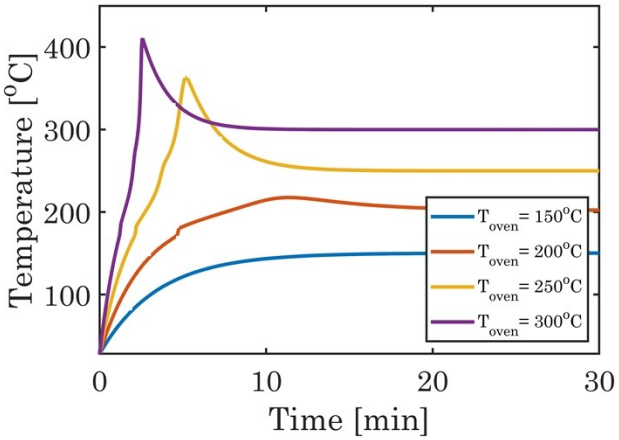

Figure SF9. Temperature vs. time profiles for the simulated 1 Ah NVP-μ-Sn-based full cell in pouch format under different oven temperatures.

Figure SF9 depicts the 1 Ah pouch cell temperature response under convective heating conditions with oven temperatures of 150°C, 200°C, 250°C and 300°C. Under convective heating conditions, the NVP-Sn-based pouch cell of 1 Ah does not experience thermal runaway for oven temperatures

of 150°C and 200°C, although there is an increase in cell temperature under heat release from Sn anode-centric exothermic reactions at 200°C. The cell experiences thermal runaway at oven temperatures of 250°C and 300°C, where the heat released from the Sn anode, as well as NVP cathode-centric exothermic reactions, cause a steep rise in the cell temperature. Under exothermic heat release, the cell temperature is seen to hike up to almost 410°C for the oven temperature of 350°C. The pouch cells employ the Whatman GF/C separator, which is reported to withstand temperatures up to 500°C, and therefore, the occurrence of internal short circuits due to separator melting does not happen. The thermal stability and safety characteristics of NVP-Sn-based pouch cells for different capacities can be evaluated based on the thermal model presented for a given cell capacity. Cell capacity varies as cells with different form factors are usually employed in various applications.

S3. Future Work

Future work for this study will include impedance testing through electrochemical impedance spectroscopy (EIS), an essential tool for getting critical insights into charge transfer resistance, SEI resistance, diffusivity, etc., to understand the effectiveness of electrolyte additives. In our previous study, we utilized EIS to investigate the effect of fluoroethylene carbonate (FEC) on μ-Sn based electrodes. Our results indicated that the size of the semi-circles related to SEI resistance significantly shrank in the presence of FEC compared to propylene carbonate (PC). This observation suggests the formation of a more stable, homogeneous, and thinner SEI layer when FEC is included in the electrolyte.[1] Similarly, for NVP, earlier research found that adding FEC reduces the overall resistance of the cell.[2] In addition, gas analysis through Differential Electrochemical Mass Spectrometry (DEMS) is a valuable tool for gaining a deeper understanding of thermal behavior and electrochemical processes. Given the strong dependence of gas evolution and SEI formation on the choice of electrolyte solvent, DEMS would allow for real-time observation of gas evolution during electrochemical reactions. This can provide immediate feedback on the processes occurring at the electrodes, helping to identify reaction intermediates and end products. For example, the electrolyte solvents used in our study, such as ethylene carbonate (EC), propylene carbonate (PC), and diethyl carbonate (DEC), exhibit different behaviors. Previous research has demonstrated that the major difference between EC and PC in gas evolution during electrochemical reactions lies in the products formed and their subsequent

impact on electrode performance. EC primarily evolves ethylene (C_2H_4), leading to a more stable SEI that enhances passivation and cycling stability. In contrast, PC produces higher gas levels, including larger amounts of propylene (C_3H_6) and heavier products, contributing to a less stable SEI that can dissolve over time.[3] These differences in gas evolution significantly affect the efficiency and overall performance of the cell. The situation is further complicated by additional gas evolution, such as CO_2 and H_2, when additives such as FEC are added to the electrolyte.[4] Therefore, conducting this analysis with DEMS will be an interesting direction for future work.

References:

1. S. Sarkar and P. P. Mukherjee, *Energy Storage Mater.*, 2021, **43**, 305-316.
2. T. Melin, R. Lundström and E. J. Berg, *Advanced Materials Interfaces*, 2021, **9**.
3. A. Schiele, B. Breitung, T. Hatsukade, B. B. Berkes, P. Hartmann, J. Janek and T. Brezesinski, *ACS Energy Letters*, 2017, **2**, 2228-2233.
4. K. Zhang, X. Zhang, W. He, W. Xu, G. Xu, X. Yi, X. Yang and J. Zhu, *Journal of Materials Chemistry A*, 2019, **7**, 9890-9902.